www.ietdl.org

Published in IET Microwaves, Antennas & Propagation
Received on 8th June 2010
Revised on 8th July 2011
doi: 10.1049/iet-map.2010.0238

ISSN 1751-8725

Compact dual-passband microstrip bandpass filters with larger design flexibility and multi-spurious suppression

L.-M. Chang[1] *M. Jiang*[2]

[1]*Department of Electronics Engineering and Institute of Electronics, National Chiao-Tung University, Hsinchu, Taiwan*
[2]*Department of Computer and Communication Engineering, Ta Hwa Institute of Technology, Hsinchu, Taiwan*
E-mail: u8913563@gmail.com

Abstract: Compact folded stepped impedance resonators (SIRs) with a novel asymmetric structure are used to design dual-passband filters with multi-spurious suppression. A complete design procedure enhancing both overall design flexibility and suppressing spurious responses is detailed. The new asymmetric SIR structure can effectively increase the degree of freedom (DOF) in the dual-passband bandwidth design. Extra DOF is simultaneously incorporated so that transmission zeros of the coupling stages may be adjusted to suppress unwanted spurious responses. Owing to circuit symmetry and a short coupling length, the circuit can be easily folded and the size is decreased by 62% compared with the previous work. The measured results agree well with the simulation and show that the attenuation level of the upper stopband is greater than 30 dB up to more than 20 GHz ($8.16f_0$).

1 Introduction

To enhance system functionality, dual-band or even tri-band operation for radio frequency (RF) devices has become important in recent wireless communication systems. A hair-pin bandpass filter designed at 2.4 and 5.2 GHz was used in a dual-band transceiver in [1]. In recent years, multiband filters have been investigated extensively and proposed [2–11]. Some have become key components in the front end of wireless communication systems. All these microwave dual-band filters suffer from unwanted higher order spurious responses, which deteriorates the rejection levels and bandwidth of the upper stopband and can greatly limit their applications. Many techniques have been proposed to tackle this problem for the single-passband filter [12–14], but very little has been done for the dual-band one. One may intuitively think that these techniques can be directly applied to suppress the spurious responses of dual-band filters without any difficulty, although in practice this may not be the case [15]. The idea in [12] was adopted to suppress the higher order spurious responses of the compact miniaturised hair-pin dual-passband filters described in [8]. The design idea in [12] for multi-spurious suppression is to stagger the higher order resonant frequencies of the constitutive stepped impedance resonator (SIRs) in a bandpass filter. Since the ratio of the leading two resonant frequencies of the dual-passband filter in [15] must be fixed, the tuning ranges of the higher order resonant frequencies of the constitutive SIRs are greatly limited. Thus, the rejection level of the upper stopband is degraded. Kuo and Lin [16] successfully used dissimilar SIRs to improve upper stopband performance, but the bandwidth design is limited by the tunings of the zeros and the circuit size is still large.

In this paper, a more compact dual-passband filter, which shows greater design flexibility while still maintaining good electrical performance, is presented. Under the condition of stationary impedance ratio and length ratio, the line width of SIR can provide an extra freedom for bandwidth determination in the two passbands [17]. The transmission zeros can then be adequately located by tuning the coupling lengths of coupled stages to effectively suppress the unwanted spurious responses. Meanwhile, a novel asymmetric SIR structure can further extend the degree of freedom in the bandwidth design [18]. Unlike [18], a detailed design procedure will be included here. Moreover, owing to circuit symmetry and short coupling length, one may easily fold the resonators such that the circuit size can be reduced by more than 62% compared with previous work, which facilitates overall circuit miniaturisation.

2 Design flexibility enhancement

Fig. 1 plots the frequency responses of both uniform impedance resonator (UIR) and SIR coupled stages with the same coupling length ℓ for comparison. It can be shown that both UIR and SIR coupled stages possess inherent transmission zeros. Besides, the transmission zero of the SIR has an even better attenuation level. As depicted in Fig. 2, the location of the transmission zero can be shifted from 4.8 to 15 GHz by varying the coupling length ℓ from 27 to 9.7 mm. Therefore the spurious responses of a

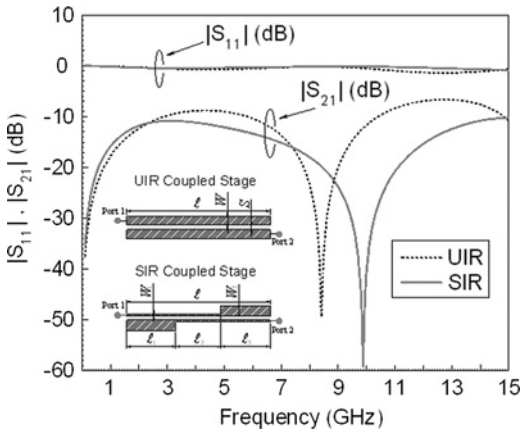

Fig. 1 *Frequency responses of UIR and SIR coupled stages for comparison*

Both circuits are simulated on a substrate with a dielectric constant $\varepsilon_r = 2.2$ and thickness $h = 0.508$ mm. (UIR coupled stage: $W = 0.54$, $S = 0.4064$, $\ell = 15.659$. SIR coupled stage: $W_1 = 0.2032$, $W_2 = 1.1062$, $\ell_1 = \ell_3 = 5.3519$, $\ell_2 = 4.9552$. Unit: mm)

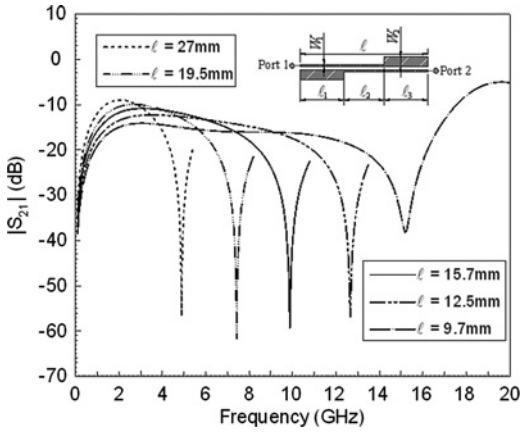

Fig. 2 *Transmission zeros of SIR coupled stages with different coupling lengths on a substrate with a dielectric constant $\varepsilon_r = 2.2$ and thickness $h = 0.508$ mm*

$W_1 = 0.2032$, $W_2 = 1.1062$, $\ell_1 = \ell_3 = 5.3519$. Unit: mm

dual-passband filter composed of parallel coupled SIRs can be effectively suppressed by adequately designing the coupling length ℓ of each coupled stage. However, once the coupling length ℓ is used to determine the position of attenuation pole, another parameter must be found to provide an additional freedom for fractional bandwidth design of the dual-passband filter in [9]. The line width of the SIR could be a suitable alternative. Nevertheless, keeping the resonant characteristic of a SIR stationary as its line width is varied is problematic. As derived in [14], the impedance ratio $R = Z_2/Z_1$ and length ratio $u = \theta_2/(\theta_1 + \theta_2)$ govern the resonant condition of a SIR. If the two key factors can be kept invariant, the influence of the line width variation on the SIR property can be neglected theoretically. Simulated frequency responses of the SIRs with identical impedance and length ratios but different line widths (line impedances) are derived using the commercial full-wave electromagnetic (EM) simulator IE3D and plotted in Fig. 3. The impedance and length ratios (R and u) are fixed to be 0.4 and 0.5, respectively, and three line widths corresponding to different impedance values (Z_1) are

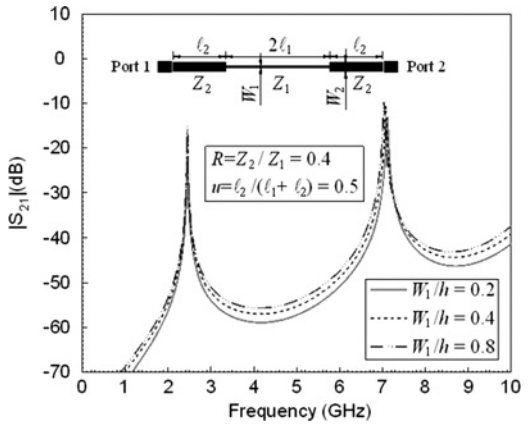

Fig. 3 *Frequency responses of SIRs with identical impedance and length ratios but different line widths*

Substrate parameters: dielectric constant $\varepsilon_r = 2.2$ and thickness $h = 0.508$ mm

adopted. It can be verified that the resonant characteristic of a SIR is almost irrelevant to the line width variation as soon as the impedance and length ratios are kept stationary. Consequently, the line widths of SIRs can provide the required freedom for bandwidth design while the lengths of coupled stages are used to locate transmission zeros for spurious suppression.

3 Design procedure

The systematic design procedure of the dual-passband filter can be mainly divided into three portions. First, the structural parameters of the constitutive SIRs including impedance ratio R and length ratio u must be determined. Then, in order to settle the coupling scheme of each coupled stage, the fractional bandwidth design graph considering both passbands must be found. Lastly, the tapped-line input/output position and dual-frequency impedance transformer should be decided.

3.1 Determination of SIR parameters

The resonant characteristics of a SIR in Fig. 3 are controlled by the following well-known transcendental equations [14]

$$\tan\theta_1 \cdot \tan\theta_2 = R, \text{ odd mode} \quad (1)$$

$$\cot\theta_1 \cdot \tan\theta_2 = -R, \text{ even mode} \quad (2)$$

where θ_1 and θ_2 are electrical lengths of the microstrip segments with characteristic impedances Z_1 and Z_2, and $R = Z_2/Z_1$ is the impedance ratio of the SIR. Suppose that we aim at designing a dual-passband filter which functions at 2.45 and 5.8 GHz, then the length and impedance ratios of the SIR must be chosen so that the frequency ratio of the leading two resonances $f_1/f_0 = 5.8/2.45 = 2.367$. The higher resonances (f_2, f_3, ...) are expected to be as far away from the fundamental mode (f_0) as possible to achieve a better upper stopband performance. The curves in Fig. 4 reveal the frequency ratios of the higher order resonances to the fundamental mode of SIRs with various impedance and length ratios. Fig. 4 is useful in determining the dimensional parameters of the constitutive SIRs in a dual-passbnad filter. A horizontal line representing an f_1/f_0 value of 2.367 (5.8/2.45) is plotted in Fig. 4 and has several

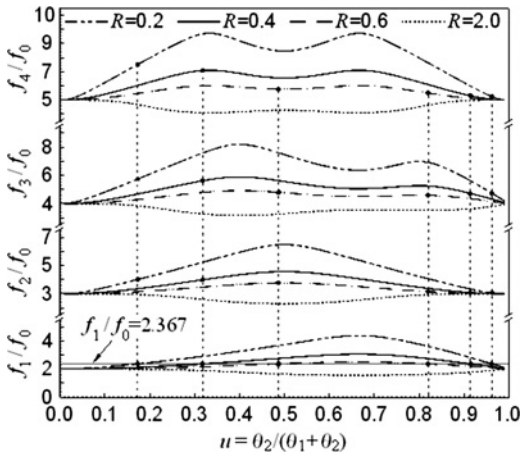

Fig. 4 *Curves of frequency ratios of the higher order resonances to the fundamental modes of SIRs corresponding to different impedance ratios $R = Z_2/Z_1$ and length ratios $u = \theta_2/(\theta_1 + \theta_2)$*

intersections with the frequency ratio curves. All these intersections provide possible candidates for the necessary SIR circuit parameters (R and u). It is worth noting in Fig. 4 that SIRs with identical f_1/f_0 ratios may have diverse frequency ratios of f_2/f_0, f_3/f_0, f_4/f_0 and so on. All the possible solutions of R and u values for $f_1/f_0 = 2.367$ form a curve (R–u curve) in Fig. 5. In addition to the R–u curve, curves of f_2/f_0, f_3/f_0 and f_4/f_0 are also included. Based on Fig. 5, smaller values of R and u corresponding to higher f_i/f_0 ($i = 2, 3, 4, \ldots$) values are beneficial for wider upper stopband. However, SIRs with very small R and u values will make circuit design and fabrication difficult. Hence, a trade-off is required.

3.2 Dual-passband bandwidth design graph

In designing a dual-passband filter systematically, the fractional bandwidth design graph is indispensable. In [9], a fractional bandwidth design graph for dual-passband filter was proposed. Nevertheless, while the suppression of higher order resonances must be taken into consideration, the establishment process of design graph would become more complicated. Instead of gap size d and coupling length ℓ of the SIR coupled stage in [9], as shown in Fig. 6, the line width W_1 and gap size S provide two freedoms for bandwidth design while the coupling length ℓ_{ov} is responsible for positioning the frequency of the

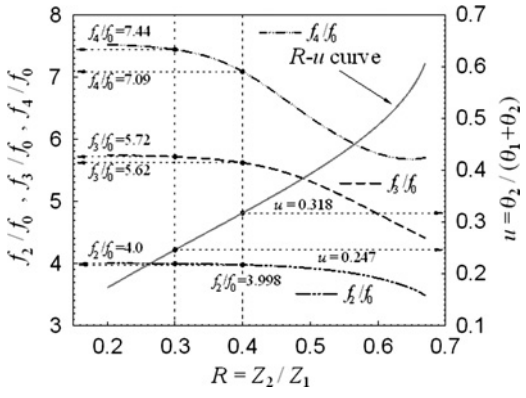

Fig. 5 *Design curves for determining R and u values of SIRs with $f_1/f_0 = 2.367$*

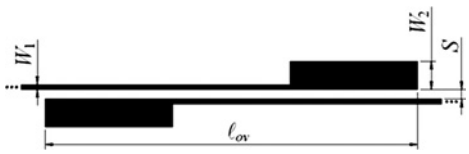

Fig. 6 *Layout of the SIR coupled stage*

transmission zero. It must be noted that the line width W_2 is varied with W_1 according to the stabilised impedance ratio R. Before building up the design graph, the operating frequencies (f_0 and f_1) and SIR parameters (R and u) must be determined in advance. Here we provide a detailed example to illustrate the determination of values of f_0 and f_1 of the SIR. Consider the SIR structure in Fig. 3; as long as the values of R and u of the SIR are given, one may first choose the line width W_1 (usually related to the substrate thickness, e.g. $W_1/h = 0.2$) and then the impedance Z_1 can be calculated. The impedance Z_2 is obtained through $R = Z_2/Z_1$ and W_2 can be determined straightforwardly. One should then estimate the value of ℓ_1 and obtain the value of ℓ_2 through $u = \ell_2/(\ell_1 + \ell_2)$. Next, commercial EM simulation software, such as IE3D, is used to simulate the SIR response. At this stage, the inaccuracy of f_1/f_0, f_0 and f_1 may be unavoidable but two key steps for fine adjustment may help one to find the desired value exactly. One can fix W_1 and slightly adjust W_2 to meet the required value of f_1/f_0; the other is to adjust the lengths ℓ_1 and ℓ_2 while fixing u (i.e. the ratio of them) to make f_0 and f_1 meet the desired values. These two steps are repeated several times. One may obtain the desired values of f_0 and f_1 precisely. The coupling coefficient C of any two adjacent SIRs can be obtained by the method used in [14]. Before deriving the coupling coefficient of a coupled stage with certain W_1 and S values, the coupling length ℓ_{ov} must be determined in advance for positioning the transmission zero at the frequency of spurious response expected to be suppressed. An Nth-order filter is composed of N resonators. The coupling coefficients for the kth band between the nth and $(n + 1)$th resonators, denoted as $(C_{n,n+1})_k$, can be derived as in [19]. The dual-band fractional bandwidth design graph can then be found.

3.3 Tapped input/output and impedance transformer

The final step is to determine the form of power input/output. A tapped-line input is adopted at end resonators of the filter as indicated in Fig. 7. From Equations (6) through (9) in [9], the tap position x can be determined once the filter specifications (Δ_k, g_{ik}) are given, where Δ_k refers to the fractional bandwidth of the kth band and g_{ik} denotes the ith prototype element value for the kth band. Based on Equations (7) and (8) in [9], then the required load impedances R_{L1} and R_{L2} can be derived. The

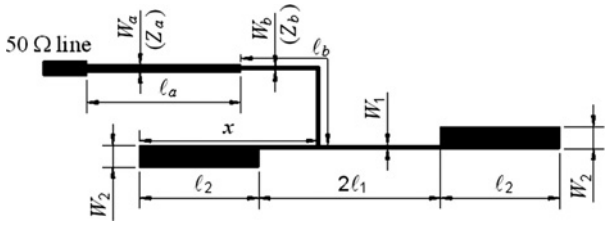

Fig. 7 *Layout of the tapped-input SIR*

doi: 10.1049/iet-map.2010.0238

design method for a dual-band impedance transformer in [20] can be used to realise R_{L1} and R_{L2}, respectively.

4 Filter design, simulation and measurement

A Chebyshev dual-passband filter centred at 2.45 GHz (f_0) and 5.8 GHz (f_1) with suppression of spurious responses was designed and fabricated. A third-order filter with traditional SIR structure has been reported in [17]. However, a filter with smaller circuit size, wider upper stopband and higher passband selectivity is always desired. Hence, a fifth-order folded filter with asymmetric SIRs is chosen to demonstrate the proposed ideas in this paper.

4.1 Novel asymmetric SIR structure

A dual-passband filter utilising asymmetric SIR structure has been reported in our previous work [18]. The comparison between a traditional SIR and novel asymmetric SIR is plotted in Fig. 8. The input impedance $Z_{in} = 1/Y_{in} = 1/(Y_\ell + Y_r)$ seen at the centre of the SIR in Fig. 8*b* can be derived. The resonant conditions for odd mode ($Z_{in} = 0$) and even mode ($Z_{in} = \infty$) can be collated as

$$\begin{cases} \tan\theta_{1\ell} \cdot \tan\theta_{2\ell} = R_\ell \\ \tan\theta_{1r} \cdot \tan\theta_{2r} = R_r \end{cases} \quad \text{odd mode} \tag{3}$$

$$\begin{cases} \cot\theta_{1\ell} \cdot \tan\theta_{2\ell} = -R_\ell \\ \cot\theta_{1r} \cdot \tan\theta_{2r} = -R_r \end{cases} \quad \text{even mode} \tag{4}$$

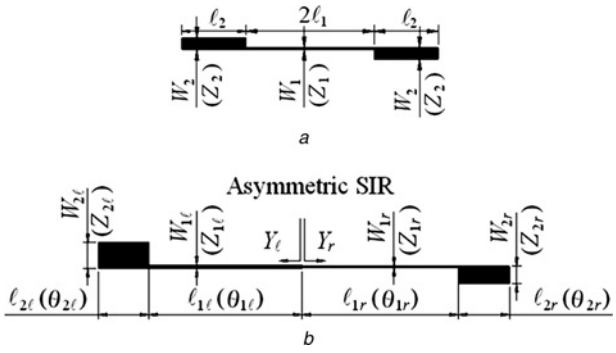

Fig. 8 *Circuit layouts*

a Traditional SIR
b Asymmetric SIR

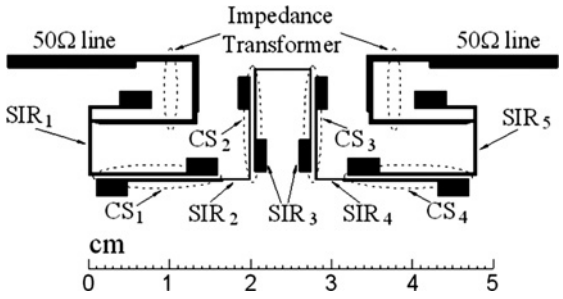

Fig. 9 *Layout of a compact folded fifth-order dual-passband filter with suppression of spurious responses*

$SIR_1(SIR_5)$: $W_a = 0.753$, $W_b = 0.4606$, $W_1 = 0.3155$, $W_2 = 2.1436$, $\ell_1 = 11.8955$, $\ell_2 = 3.902$, $x = 9.212$. $SIR_2(SIR_4)$: $W_{1\ell} = 0.3155$, $W_{2\ell} = 2.1273$, $W_{1r} = 0.1417$, $W_{2r} = 1.4802$, $\ell_{1\ell} = 11.7145$, $\ell_{2\ell} = 3.8426$, $\ell_{1r} = 12.02$, $\ell_{2r} = 3.9428$. SIR_3: $W_1 = 0.1417$, $W_2 = 1.4579$, $\ell_1 = 12.0705$, $\ell_2 = 3.9594$. $CS_1(CS_4)$: $\ell_{ov} = 14.9775$, $S = 0.4068$. $CS_2(CS_3)$: $\ell_{ov} = 11.6855$, $S = 0.5447$. Unit: mm

where $R_\ell = Z_{2\ell}/Z_{1\ell}$ and $R_r = Z_{2r}/Z_{1r}$. Letting $\theta_{1\ell} = \theta_{1r} = \theta_1$, $\theta_{2\ell} = \theta_{2r} = \theta_2$ and $R_\ell = R_r = R$, (1) and (2) can be simplified to the form of the resonance conditions for traditional SIRs as in [14]. In other words, as long as the above conditions are held, the line widths of the asymmetric SIR can be arbitrarily changed without affecting the SIR resonant characteristics. Hence, the degree of freedom in the bandwidth design of the filter can be effectively increased.

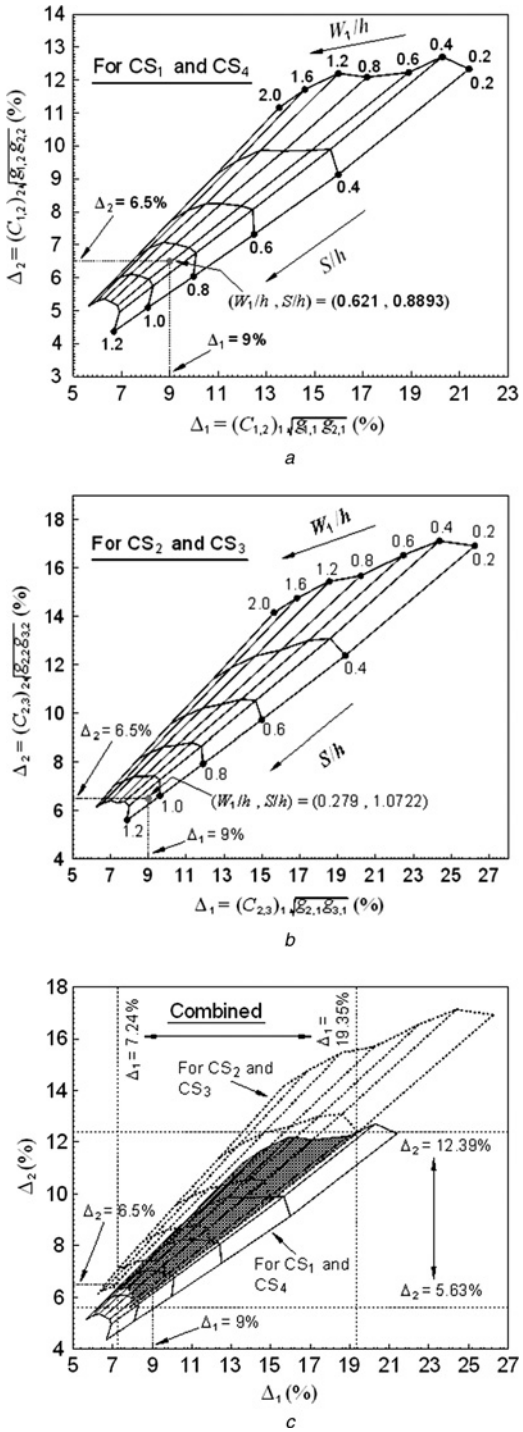

Fig. 10 *Fractional bandwidth design graphs for a fifth-order dual-passband filter with suppression of spurious responses*

a Design graph for CS_1 and CS_4
b Design graph for CS_2 and CS_3
c Combined version of *a* and *b*

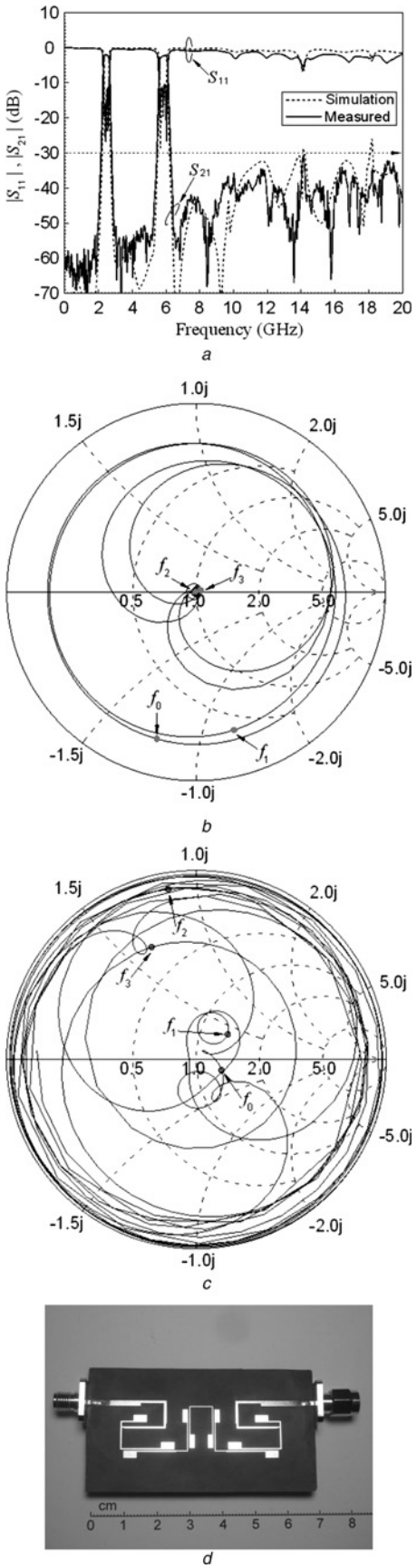

Fig. 11 *Frequency response, Smith chart, and photograph*

a Simulation and measured frequency responses of the experimental folded dual-passband bandpass filter with order $N = 5$

b Smith chart of measured two-port S_{21} for the filter

c Smith chart of measured two-port S_{11} for the filter. All from 0 to 20 GHz. ($f_0 = 2.45$ GHz, $f_1 = 5.8$ GHz, $f_2 = 9.8$ GHz, $f_3 = 14.01$ GHz)

d Photograph of the fabricated filter

4.2 Folded fifth-order dual-passband filter

The design example of a third-order dual-passband filter was given in [17]. A bandpass filter with higher order can not only enhance the passband selectivity but also possess more coupled stages to produce transmission zeros for harmonics suppression, but the circuit size is inevitably larger. However, when assessing the applicability of any technique at an industrial level, circuit size reduction is always desirable. A folded structure is one of the most intuitive solutions and can be illustrated by a fifth-order dual-passband filter. Owing to structure symmetry and short coupling length, circuit miniaturisation is excellent (the size is decreased significantly compared with the previous works [16, 18]) as shown in Fig. 9, consisting of five folded resonators (SIR_1–SIR_5) and four coupled stages (CS_1–CS_4). Two coupled stages CS_1 and CS_4 are expected to suppress the spurious response at f_2 while CS_2 and CS_3 are used to cope with the unwanted harmonic at f_3. Owing to the fact that different coupled stages may need diverse line widths, the second and fourth resonators in Fig. 9 adopt the asymmetric SIR structure discussed above.

Based on the discussion in Section 4.1, the fractional bandwidth design graph for each coupled stage can be founded independently. Following the filter design procedure in Section 3, an impedance ratio $R = 0.3$ was first chosen from Fig. 5. The corresponding values of u, f_2/f_0, f_3/f_0 and f_4/f_0 are 0.247, 4.0, 5.72 and 7.44, respectively. The spurious responses at f_2 and f_3 are expected to be suppressed by coupled stages (CS_1–CS_4) and the upper stopband can be extended to $7.44f_0$ theoretically. Then, the fractional bandwidth design graph must be established. The passband ripples for the first and second passband are 0.01 and 0.1 dB, respectively. The corresponding element values of the low-pass filter prototype are $g_{1,1} = g_{5,1} = 0.7563$, $g_{2,1} = g_{4,1} = 1.3049$, $g_{3,1} = 1.5773$, $g_{1,2} = g_{5,2} = 1.1468$, $g_{2,2} = g_{4,2} = 1.3712$ and $g_{3,2} = 1.975$. The design graph can be divided into two portions. The design graph in Fig. 10*a* is for coupled stages CS_1 and CS_4 and that in Fig. 10*b* is for CS_2 and CS_4. The transmission zeros of the coupled stages in Fig. 10*a* are positioned at f_2 ($4f_0$), while those in Fig. 10*b* are at f_3 ($5.72f_0$). The combined version is shown in Fig. 10*c*. The shadow region in Fig. 10*c* represents the realisable fractional bandwidth region for both bands in the given circuit size range of W_1/h and S/h. The range of Δ_1 is from 7.24 to 19.35%, and that of Δ_2 is between 5.63 and 12.39%. The range of the realisable

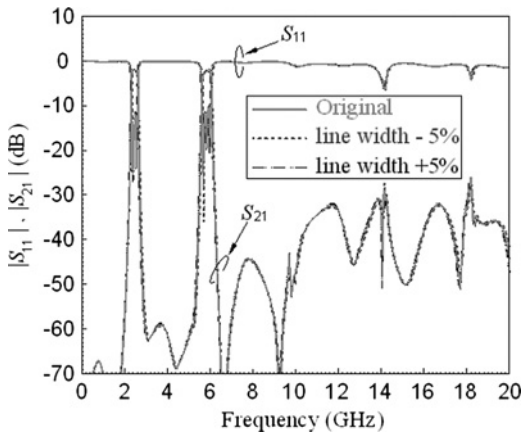

Fig. 12 *Comparison of simulated responses for three different etching results*

doi: 10.1049/iet-map.2010.0238

Table 1 Simulated scattering parameters at some critical frequencies (dB)

	$\|S_{11}\|$ @ f_0	$\|S_{11}\|$ @ f_1	$\|S_{21}\|$ @ f_0	$\|S_{21}\|$ @ f_1	$\|S_{21}\|$ @ f_2	$\|S_{21}\|$ @ f_3
case 1	−11.76	−10.76	−1.853	−2.064	−43.24	−28.6
case 2	−11.37	−9.646	−1.929	−2.207	−46.63	−27.37
case 3	−12.08	−11.30	−1.793	−1.908	−43.24	−29.94

fractional bandwidth region for both bands in Fig. 10*c* can be adjusted by the element values of the low-pass filter prototype. Based on Figs. 10*a*–*c*, Δ_1 and Δ_2 are chosen to be 9 and 6.5%, respectively. The corresponding coupled stage circuit sizes (W_1/h, S/h) for CS_1 and CS_4 are (0.621, 0.8893), and those for CS_2 and CS_3 are (0.279, 1.0722). The next step is to determine the position of the tapped-line input/output. Using a method similar to that in [9], appropriate values of $x/(2\ell_1 + 2\ell_2)$ in Fig. 7 for $\Delta_1/\Delta_2 = 0.09/0.065 = 1.385$ can be 0.288 or 0.712. The necessary load impedances, R_{L1} and R_{L2}, have an identical value of 153.3 Ω. The dual-band frequency transformer has dimensions $Z_a = 77.6\ \Omega$, $Z_b = 98.8\ \Omega$, $\ell_a = \ell_b = 13.59$ mm. The fifth-order dual-passband filter is also fabricated on a high-frequency laminate (RT/duroid® 5880) with $\varepsilon_r = 2.2$ and $h = 0.508$ mm. The RF measurement was performed using an Agilent 8510C network analyser. In order to achieve more accurate measured results, a thru-reflect line calibration was performed in advance. The measured and simulated frequency responses are plotted in Figs. 11*a*–*c*, and Fig. 11*d* is the photograph of the fabricated filter. The circuit layout including geometric dimensions is shown in Fig. 9 (Figs. 6, 7, 8*a*, *b*, show the dimension parameters of SIR_1 (SIR_5), SIR_2 (SIR_4), SIR_3, CS_1–CS_4, respectively). The measured and simulation frequency responses in Fig. 11*a* are in good agreement. The insertion losses at f_0 and f_1 are 1.89 and 2.13 dB, respectively, and both return losses are greater than 10.5 dB. It can be shown that the measured spurious responses at f_2 ($4.0f_0 = 9.8$ GHz) and f_3 ($5.72f_0 = 14.01$ GHz) are effectively suppressed. The upper stopband can have an attenuation level larger than 30 dB up to more than 20 GHz ($8.16f_0$). The S-parameters shown in Smith chart format in Figs. 11*b* and *c* also agree well with the designed specification. (For clarity, only the measured data is shown in the figures.) The S-parameters at f_0 and f_1 indicate typical passband characteristics while those at f_3 and f_4 show high reflection. Including impedance transformers, the layout area of the proposed compact folded filter shown in Fig. 9 is 47.97 mm × 15.67 mm. Compared with the fifth-order filter in [18] (126.26 mm × 18.1 mm), the length is decreased by 62% and area by 67%.

4.3 Influences caused by process variation

Any fabrication process will unavoidably introduce design parameter variability in the manufacturing stage. Owing to the use of a standard print circuit board etching process, to analyse the influence caused by the process variation effect, that is, over- or under-etching, we use the full-wave EM simulator IE3D [21] to examine the influences through varying the line width of the overall circuit.

We categorise the situation into three different cases and compare the differences between each other. Case 1 represents the simulated result of originally designed circuit. Case 2 and Case 3 are that of the circuit with line width decreased by 5% (over-etching) and with line width increased by 5% (under-etching), respectively. The simulation results, inclusive of scattering parameters at some critical frequencies (S_{11} at f_0, f_1, and S_{21} at f_0, f_1, f_2, f_3) of the three cases, are shown in Fig. 12 and summarised in Table 1. According to Fig. 12 and Table 1, it is found that the influence of line width change caused by slight etching variation on the overall frequency response is not significant.

5 Conclusion

A complete design methodology for microstrip line folded dual-passband filters with greater design flexibility and multi-spurious suppression has been developed. Three key ideas are introduced in this paper. First, the SIR coupled stage can have essential transmission zeros with even better attenuation than the UIR one. Second, the method for changing the line width of SIR but keeping the SIR resonant characteristic invariant is presented, which provides the required freedom for bandwidth design while the lengths of coupled stages are used to locate transmission zeros for spurious suppression. Third, an asymmetric SIR structure can further extend the bandwidth design flexibility. Based on these ideas, the fractional bandwidth design graphs giving consideration to the positions of the transmission zeros of constitutive coupled stages can be established. In addition, as long as circuit symmetry and short coupling lengths are maintained, the circuit layout optimisation can be easily achieved by folding. Consequently, one can conveniently design a compact dual-passband filter with improved upper stopband performance. An experimental filter is designed and fabricated to validate the proposed ideas. The circuit size is decreased by more than 60%. Based on the measured responses, the fifth-order filter can have an upper stopband with an attenuation level greater than 30 dB up to more than $8.16f_0$. Finally, the simulation results show that the influence caused by the process variation effect on the filter performance is not significant.

6 Acknowledgments

This work was supported in part by National Nano Project NSC 97-2120-M-009-005 and NSC 97-2221-E-233-002 of Taiwan. The authors especially thank Prof. Jen-Tsai Kuo and Prof. Shyh-Jong Chung, Department of Communications Engineering, National Chiao Tung University, Taiwan, ROC, for their valuable comments and assistance with measurements.

7 References

1 Chang, S.-F.R., Chen, W.-L., Chang, S.-C., *et al.*: 'A dual-band RF transceiver for multistandard WLAN applications', *IEEE Trans. Microw. Theory Tech.*, 2005, **53**, (3), pp. 1048–1055
2 Macchiarella, G., Tamiazzo, S.: 'Design techniques for dual-passband filters', *IEEE Trans. Microw. Theory Tech.*, 2005, **53**, (11), pp. 3265–3271
3 Mokhtaari, M., Bornemann, J., Rambabu, K., Amari, S.: 'Coupling-matrix design of dual and triple passband filters', *IEEE Trans. Microw. Theory Tech.*, 2006, **54**, (11), pp. 3940–3946

4 Lee, J., Sarabandi, K.: 'A synthesis method for dual-passband microwave filters', *IEEE Trans. Microw. Theory Tech.*, 2007, **55**, (6), pp. 1163–1170
5 Lee, H.-M., Tsai, C.-M.: 'Dual-band filter design with flexible passband frequency and bandwidth selections', *IEEE Trans. Microw. Theory Tech.*, 2007, **55**, (5), pp. 1002–1009
6 Lee, J., Uhm, M.S., Yom, I.-B.: 'A dual-passband filter of canonical structure for satellite applications', *IEEE Microw. Wirel. Compon. Lett.*, 2004, **14**, (6), pp. 271–273
7 Chen, C.-Y., Hsu, C.-Y.: 'A simple and effective method for microstrip dual-band filters design', *IEEE Microw. Wirel. Compon. Lett.*, 2006, **16**, (5), pp. 246–248
8 Kuo, J.-T., Cheng, H.-S.: 'Design of quasi-elliptic function filters with a dual-passband response', *IEEE Microw. Wirel. Compon. Lett.*, 2004, **14**, (10), pp. 472–474
9 Kuo, J.-T., Yeh, T.-H., Yeh, C.-C.: 'Design of microstrip bandpass filters with a dual-passband response', *IEEE Trans. Microw. Theory Tech.*, 2005, **53**, (4), pp. 1331–1337
10 Sun, S., Zhu, L.: 'Compact dual-band microstrip bandpass filter without external feeds', *IEEE Microw. Wirel. Compon. Lett.*, 2005, **15**, (10), pp. 644–646
11 Weng, M.-H., Wu, H.-W., Su, Y.-K.: 'Compact and low loss dual-band bandpass filter using pseudo-interdigital stepped impedance resonators for WLANs', *IEEE Microw. Wirel. Compon. Lett.*, 2007, **17**, (3), pp. 187–189
12 Chen, C.-F., Huang, T.-Y., Wu, R.-B.: 'Design of microstrip bandpass filters with multiorder spurious-mode suppression', *IEEE Trans. Microw. Theory Tech.*, 2005, **53**, (12), pp. 3788–3793
13 Jiang, M., Wu, M.-H., Kuo, J.-T.: 'Parallel-coupled microstrip filters with over-coupled stages for multispurious suppression'. IEEE MTT-S Int. Microwave Symp. Digest, Long Beach, California, USA, June 2005, pp. 687–690
14 Kuo, J.-T., Shih, E.: 'Microstrip stepped impedance resonator bandpass filter with an extended optimal rejection bandwidth', *IEEE Trans. Microw. Theory Tech.*, 2003, **51**, (5), pp. 1554–1559
15 Jiang, M., Lin, H.-P., Kuo, J.-T.: 'Design of quasi-elliptic function filters with dual-passband responses and multi-spurious suppression'. Proc. Asia-Pacific Microwave Conf., Bangkok, Thailand, December 2007, pp. 2365–2368
16 Kuo, J.-T., Lin, H.-P.: 'Dual-band bandpass filter with improved performance in extended upper rejection band', *IEEE Trans. Microw. Theory Tech.*, 2009, **57**, (4), pp. 824–830
17 Jiang, M., Chang, L.-M., Chin, A.: 'Design of dual-passband microstrip bandpass filters with suppression of higher order spurious response'. Proc. Asia-Pacific Microwave Conf., Singapore, December 2009, pp. 2060–2063
18 Jiang, M., Chang, L.-M., Chin, A.: 'Design of dual-passband microstrip bandpass filters with suppression of higher order spurious response', *IEEE Microw. Wirel. Compon. Lett.*, 2010, **20**, (4), pp. 199–201
19 Mattaei, G.L., Young, L., Jones, E.M.T.: 'Microwave filters, impedance-matching network, and coupling structures' (Artech House, 1980)
20 Monzon, C.: 'A small dual-frequency transformer in two sections', *IEEE Trans. Microw. Theory Tech.*, 2003, **51**, (4), pp. 1157–1161
21 Zeland Software, Inc., IE3D Simulator, January 1997

doi: 10.1049/iet-map.2010.0238